metals

MDPI

Article

Acid and Acid-Alkali Treatment Methods of Al-Chloride Solution Obtained by the Leaching of Coal Fly Ash to Produce Sandy Grade Alumina

Dmitry Valeev [1,2,*], Andrei Shoppert [3], Alexandra Mikhailova [4] and Alex Kondratiev [2]

1 Laboratory of New Metallurgical Processes, A.A. Baikov Institute of Metallurgy and Materials Science, Russian Academy of Sciences, 49, Leninsky Prospect, 119334 Moscow, Russia
2 Scientific Research Centre "Thermochemistry of Materials", National University of Science & Technology "MISIS", 4, Leninsky Prospect, 119049 Moscow, Russia; al.v.kondratiev@gmail.com
3 Department of Non-ferrous Metals Metallurgy, Ural Federal University named after the first President of Russia B.N. Yeltsin, Yekaterinburg 620002, Russia; andreyshop@list.ru
4 Laboratory of Crystal Structure Studies, A.A. Baikov Institute of Metallurgy and Materials Science, Russian Academy of Sciences, 49, Leninsky Prospect, 119334 Moscow, Russia; sasham1@mail.ru
* Correspondence: dmvaleev@yandex.ru; Tel.: +7-905-781-6667

Received: 13 April 2020; Accepted: 28 April 2020; Published: 29 April 2020

Abstract: Sandy grade alumina is a valuable intermediate material that is mainly produced by the Bayer process and used for manufacturing primary metallic aluminum. Coal fly ash is generated in coal-fired power plants as a by-product of coal combustion that consists of submicron ash particles and is considered to be a potentially hazardous technogenic waste. The present paper demonstrates that the Al-chloride solution obtained by leaching coal fly ash can be further processed to obtain sandy grade alumina, which is essentially suitable for metallic aluminum production. The novel process developed in the present study involves the production of amorphous alumina via the calcination of aluminium chloride hexahydrate obtained by salting-out from acid Al-Cl liquor. Following this, alkaline treatment with further Al_2O_3 dissolution and recrystallization as $Al(OH)_3$ particles is applied, and a final calcination step is employed to obtain sandy grade alumina with minimum impurities. The process does not require high-pressure equipment and reutilizes the alkaline liquor and gibbsite particles from the Bayer process, which allows the sandy grade alumina production costs to be to significantly reduced. The present article also discusses the main technological parameters of the acid treatment and the amounts of major impurities in the sandy grade alumina obtained by the different (acid and acid-alkali) methods.

Keywords: coal fly ash; sandy grade alumina; $AlCl_3 \cdot 6H_2O$; crystallization; salting-out method; gibbsite; precipitation

1. Introduction

Sandy grade alumina (SGA) is the aluminum oxide that is used for metallic aluminum production and is mainly produced by the Bayer alkaline method. In this method, bauxite is used as a raw material, which may differ in quality and composition. For bauxite with a high silica content, the sintering process is used [1,2]. A decrease in the bauxite quality and orientation of the main aluminum producers (Russia and China) with regards to their own resources has led to investigations of alternative raw materials for SGA production [3]. In fact, it can be obtained from both natural (kaolin clay [4,5] or pyrophyllite ore [6]) and technogenic (red mud [7], coal fly ash (CFA) [8], and secondary aluminum dross [9,10]) materials. The CFA waste generated from coal-fired power plants is one of the most promising raw materials for SGA production [11], since it does not require preliminary grinding, as in

the case of using kaolin clay, or the removal of alkali, as in the case of using red mud [12]. The CFA volume produced annually varies in each country, depending on the share of coal in the electricity generation. In Russia, 25 million tons are generated annually, while only 8% was utilized in 2019. The Russian Government plans to increase this quantity to 50% by 2035 [13].

Since CFA has a low silicon modulus (the mass ratio of Al_2O_3 to SiO_2), in the range of 0.45–0.55, acid treatment (leaching) is the main approach employed to extract aluminum from CFA. Sulfuric acid (H_2SO_4) [14], ammonium bisulfate ($(NH_4)_2SO_4$) [15], potassium bisulfate ($KHSO_4$) [16], and hydrochloric acid (HCl) [17] are normally used for aluminum leaching. The use of HCl is more promising, since the chloride liquor can be used as a coagulant, polyaluminum chloride (PAC), for water treatment after leaching [18]. In addition to aluminum, valuable metals can be extracted from the liquor, including gallium (Ga) [19], scandium (Sc) [20], and rare earth elements (REE) [21], which can effectively be recovered as separate concentrates.

Various methods have been used to precipitate aluminum from acidic solutions and subsequently obtain alumina: salting-out by the addition of salts, alkali precipitation, isothermal evaporation [22], and direct spray pyrolysis of an acid solution at T = 1000 °C [23]. In the salting-out method, sodium chloride (NaCl) [24], calcium chloride ($CaCl_2$) [25], ammonium chloride (NH_4Cl), magnesium chloride ($MgCl_2$), or strontium chloride ($SrCl_2$) can be used [26]. The use of alkaline reagents, such as ammonia hydrate (NH_4OH) or sodium hydroxide (NaOH), leads to the formation of gibbsite ($Al(OH)_3$), which is accompanied, however, by an irreversible loss of hydrochloric acid [27].

The salting-out of aluminum chloride hexahydrate (ACH: $AlCl_3 \cdot 6H_2O$) performed by flushing gaseous HCl through the solution leads to a decrease in the ACH solubility and its precipitation [28]. This method is the most promising one, since it allows the reuse of hydrochloric acid and permits ACH crystals to be obtained with a minimum amount of impurities. The alkali leaching of alumina after ACH calcination is another way of providing a low impurity content.

In preceding studies [29], we have shown that coal fly ash can be utilized by HCl autoclave leaching to produce an Al-chloride solution, which can readily be used as a water coagulant. In the present study, we propose a novel method that allows sandy grade alumina suitable for the Bayer process to be produced from Al-chloride liquor, which was obtained after leaching coal fly ash. The method, for which the flowsheet is given in Figure 1, consists of two stages: first, conventional acid treatment (salting-out), and then, combined acid-alkali treatment, with intermediate calcination stages. Contrary to the conventional route (shown by red arrows), this method (shown by green arrows) provides SGA with minimum impurities, which can directly be utilized to produce primary metallic aluminum. The present article also discusses the main technological parameters of the salting-out process and the behavior of the main impurities, and compares the SGA obtained by the conventional acid and the novel acid/alkaline treatment methods.

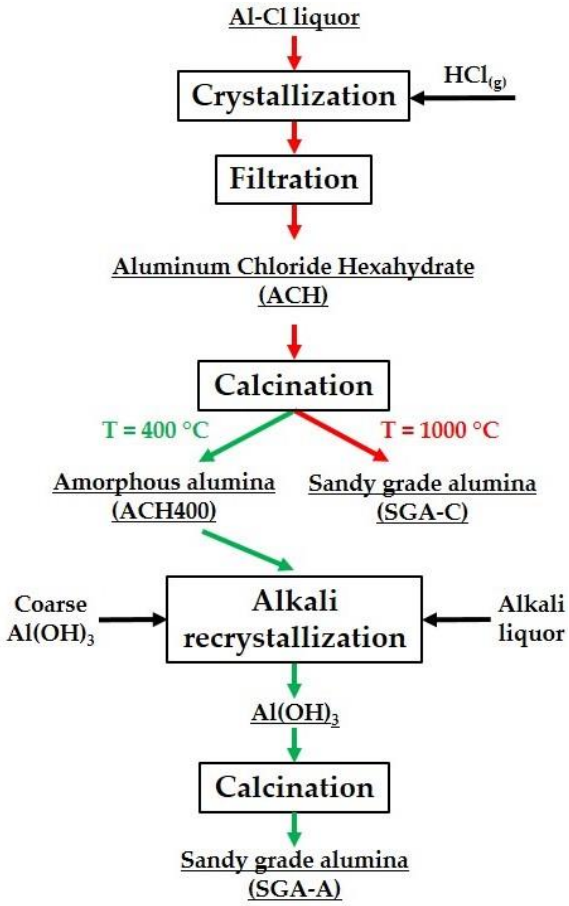

Figure 1. A flowsheet of sandy grade alumina (SGA) production from the Al-chloride liquor by the conventional acid and novel acid-alkali treatment methods (red arrows show the traditional acid method used for SGA production, and green arrows show the new acid-alkali method).

2. Materials and Methods

2.1. Materials

Raw CFA was collected from the Omsk TPP-4 ash residue storage (Google Earth coordinates: 55.129231, 73.167497). Magnetite concentrate and unburned carbon were separated from CFA by wet magnetic separation and by foam flotation with kerosene as a collector, respectively [30]. The non-magnetic fraction, after the enrichment process, was subjected to high-pressure HCl leaching to maximize the aluminum extraction from the liquor (T = 210 °C, C_{HCl} = 30%, τ = 3 h, and the solid liquid ratio = 1:5) [29]. The chemical composition of the liquor is presented in Table 1.

Table 1. The chemical composition (g/l), measured by inductively coupled plasma optical emission spectrometry (ICP-OES), of the aluminum chloride liquor obtained by high-pressure HCl leaching of coal fly ash (CFA).

Al	Ca	Fe	Ti	Na	K	Si	Sc	Cl_{total}
22.3	3.8	2.5	0.3	0.2	0.1	4.5×10^{-3}	2.2×10^{-3}	335

2.2. Analytical Methods

The metal concentrations in the liquor and solid samples were measured by inductively coupled plasma optical emission spectrometry (ICP-OES) using an atomic absorption spectrometer AA-240FS

(Varian, Belrose, Australia). Solid samples were dissolved beforehand by distilled water (ACH) or hydrochloric acid (alumina).

An X-ray diffraction analysis (XRD) of samples was carried out using an Ultima IV diffractometer (Rigaku, Tokyo, Japan) with Cu-Kα; the radiation was in a range of 2θ angles of 10–100° with a 0.02° step. The quantitative and qualitative structure of samples were investigated using the PDXL (Rigaku) program.

The change of mass and temperature of phase transformations of the ACH sample were determined via differential scanning calorimetry (DSC) and thermogravimetric analysis (TGA), using an STA 409 Luxx synchronous thermal analyzer (Netzsch, Selb, Germany) combined with a QMS 403 Aeolos quadrupole mass spectrometer with a capillary connection (Netzsch, Selb, Germany). The heating rate was 5 °C/min in the temperature range of 100–1200 °C.

The morphology of the samples was examined by scanning electron microscopy (SEM) using EVO LS 10 (Carl Zeiss, Oberkochen, Germany) and Vega 3 (Tescan, Brno, Czech Republic) microscopes.

The particle size distribution and specific surface area of the samples were determined by the laser diffraction method (LD) using an Analysette 22 NanoTec analyzer (Fritsch, Idar-Oberstein Germany) and by the Brunauer–Emmett–Teller method (BET) using a NOVA 1200e apparatus (Quantachrome Instruments, Hook, UK).

2.3. Experiments

The salting-out of ACH from the aluminum chloride liquor was carried out by the flushing of gaseous HCl mixed with Ar at a rate of 1.5 g/min (Figure 2) through a Drexel flask with 10 mL of the liquor, which was thermostated at temperatures of 0, 25, 50, 75, and 95 °C for 10 min. The ACH crystals obtained were separated from the liquor in a Schott funnel. Polypropylene, which was stable in hydrochloric acid, was used as a filter cloth, and acetone was used as a washing liquid. After washing, the ACH crystals obtained were dried in a drying oven at 105 °C for 2 h, and the impurities in the crystals were then analyzed.

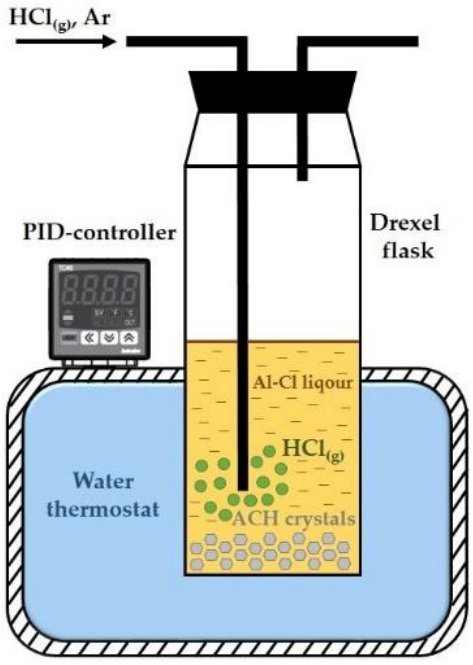

Figure 2. Schematic of the salting-out experimental set-up.

Amorphous Al_2O_3 (ACH400) was obtained by the calcination of ACH crystals in an electric tube furnace (SNOL, Moscow, Russia) in a corundum boat. The heating time to T = 400 °C was 15 min,

the weight of the ACH sample was 15 g, and the calcination time was 1 h. Exhaust gases (HCl) were passed through a Drexel flask with distilled water to regenerate HCl.

The leaching of ACH400 was carried out in a thermostatically controlled stainless-steel reactor equipped with an overhead stirrer. The alkaline aluminate liquor (500 mL) with a concentration of Na_2O_k = 150 g/L and α_k = 3.4 was loaded into the reactor. After reaching 60 °C, 200 g/L of a 2:1 mixture of aluminum hydroxide from the Ural Aluminum Smelter (coarse $Al(OH)_3$ in Figure 1) and ACH400, respectively, was added to the reactor. Then, the pulp was maintained for 36 h with constant-speed stirring of 200 rpm. The precipitate obtained was separated from the liquor by filtration, washed with hot water, and dried at 105 °C for 8 h.

The conventional SGA obtained from ACH crystals (SGA-C) and the novel SGA obtained from $Al(OH)_3$ (SGA-A) were then annealed in a muffle furnace HTC 03/18/3N/PE (Nabertherm, Lilienthal, Germany) in open corundum crucibles. The heating time to T = 1000 °C was 1 h, the weight of the sample was 5 g, and the calcination time was 1 h.

2.4. Equations

The ACH crystal size distribution was determined by an analysis of the SEM images. It was impossible to use LD analysis, since the crystals dissolve in water. The Sturges equation [31] was employed to find the number of intervals of the particle size distribution histogram (n):

$$n = 1 + 3.22 \times \text{Log}\,(N), \quad (1)$$

where N is the number of measured ACH particles.

The data obtained were analyzed by the Origin Pro 8 Software, and 1120, 790, and 813 ACH particles were determined for each ACH sample (0, 50, and 95 °C, respectively).

The ACH recovery level (R) from the aluminum chloride liquor was calculated by the following equation:

$$R = (Al_1/Al_2) \times 100\%, \quad (2)$$

where Al_1 and Al_2 represent the aluminum content (g/l) in the aluminum chloride liquor after and before salting-out experiments.

3. Results

3.1. ACH Precipitation

The temperature of the Al chloride liquor and the HCl content are the two most important parameters of the salting-out process, which affect both the precipitation of the main impurities (Fe, Ca, Na, and K) and the yield of the ACH crystals [32,33]. It was found that the temperature of the liquor does not significantly affect the ACH solubility. At 125 °C, this value was 4.012 mol/kg, and at 0 °C, it was 3.283 mol/kg [34]. The HCl concentration imposes a much greater effect: with water liquor (0 mol/kg HCl), the ACH solubility was 31.20%, while with 10 mol/kg HCl, this value decreased to 0.13%. The solubility of iron chloride hexahydrate was practically unchanged and stayed at a ~50% level [35,36]. The effect of temperature on the ACH yield is illustrated in Figure 3. Decreasing the temperature from 95 to 0 °C enhances the ACH yield from 58% to 99%, respectively.

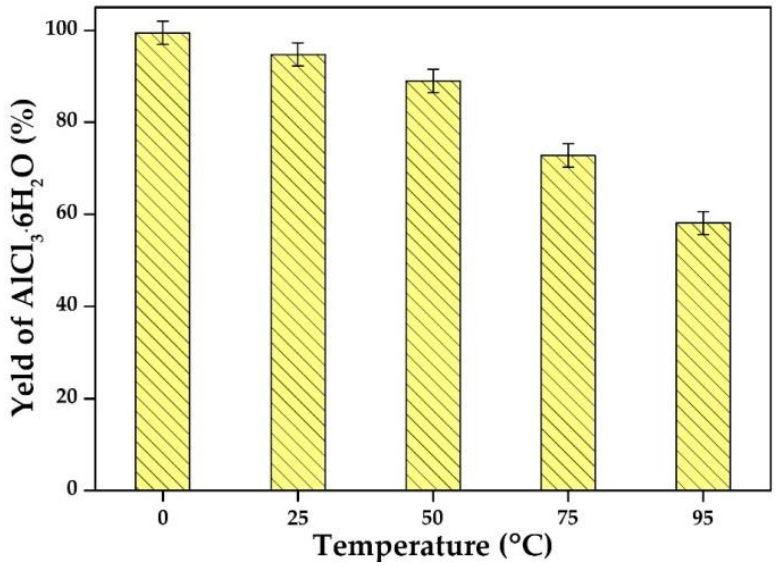

Figure 3. The effect of the aluminum chloride liquor temperature on the distilled water (ACH) yield in the salting-out process.

The dependence obtained correlates with the ACH crystal size distribution shown in Figure 4. At 95 °C, the number of small crystals ≤100 μm is significantly lower than that at 50 and 0 °C. The average crystal size for 0, 50, and 95 °C is 85, 127, and 135 μm, respectively. A large number of small crystals at 0 °C can simultaneously work as precursors for the formation of new ones.

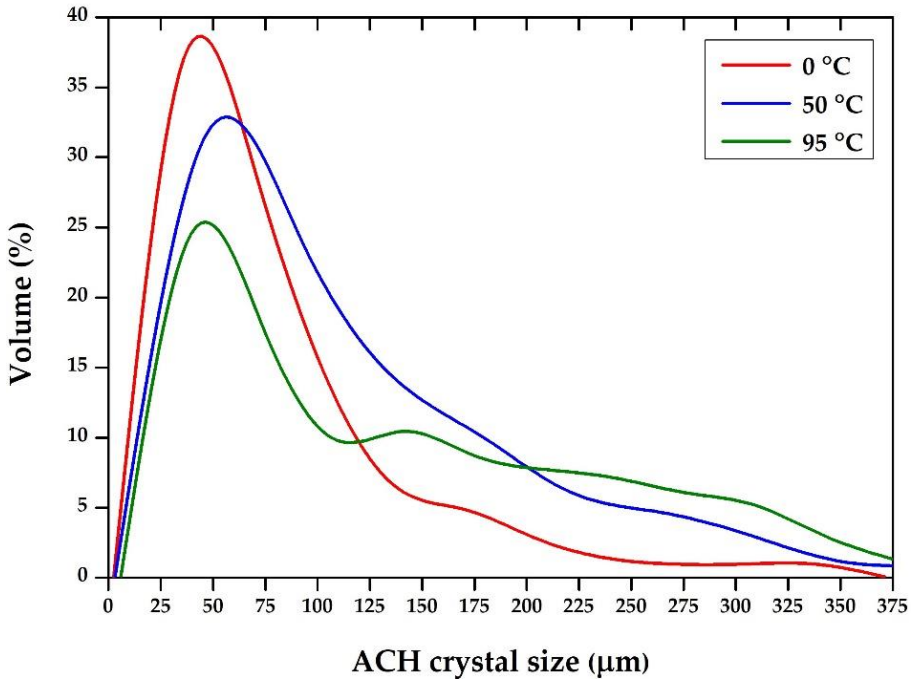

Figure 4. The crystal size distribution of ACH, obtained at 0, 50, and 95 °C.

Figure 5a–c provide the SEM images of ACH crystals obtained at different temperatures. It can be seen that the temperature greatly affects the ACH crystal size, which can be associated with a change in the supersaturation and density of the liquor caused by an increasing temperature [22,34,37]. An increase of the density, apparently, leads to a decrease in the supersaturation of the liquor at T > 50 °C and results in a lower degree of the ACH yield. With high supersaturation, the rate

of nucleation often exceeds the crystal growth rate [38,39], which accounts for the formation of smaller crystals at 0 °C (Figure 5a). However, at the surface of large crystals (>100 µm), the offset of secondary nucleation and crystallization can be observed (see Figure 5b, where yellow arrows indicate secondary crystals). This is most clearly seen in the sample obtained at 95 °C, where the sizes of the secondary crystals exceed 100 µm (Figure 5c). The secondary nucleation of gibbsite was also studied by Li et al. [40].

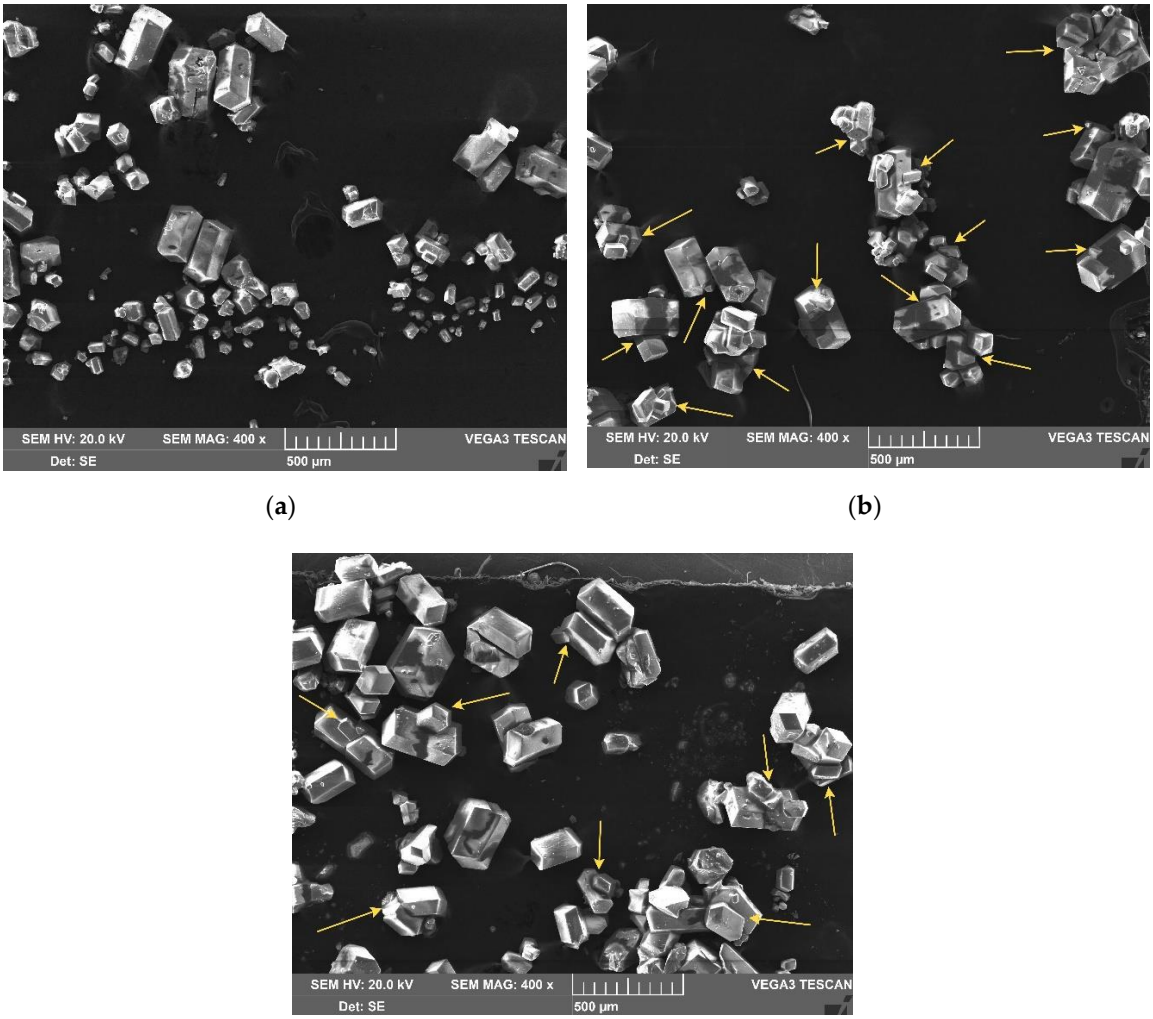

Figure 5. The SEM images of aluminum chloride hexahydrate (ACH) crystals obtained at (**a**) 0 °C, (**b**) 50 °C, and (**c**) 95 °C (yellow arrows indicate secondary nucleation and crystallization on the surface of primary crystals).

The chemical composition of the ACH crystals obtained at 0–95 °C is presented in Table 2. It can be seen that the total content of impurities in the crystals stays within a range of 0.05–0.1 wt.%. It can also be concluded from the results presented in Table 2 that a decrease of temperature of the aluminum chloride solution reduces the solubility of K, Na, and Si impurities, which was also confirmed by Gao et al. for $CaCl_2$ and KCl [41].

Table 2. The chemical composition, measured by ISP-OES, of impurities in ACH obtained at 0–95 °C (wt.%).

Salting-out Temperature	Cr	Fe	K	Mn	Na	P	Si	Ti	V	Zn
0 °C	0.0038	0.01	0.0073	0.0005	0.039	0.021	0.011	0.0075	0.00037	0.0001
25 °C	0.0020	0.0027	0.0083	0.00016	0.0075	0.017	0.013	0.0060	0.00036	0.0001
50 °C	0.0004	0.0035	0.0085	0.00007	0.0075	0.013	0.021	0.0027	0.00032	0.0001
75 °C	0.0004	0.0041	0.0091	0.0001	0.0075	0.012	0.021	0.0022	0.00027	0.0002
95 °C	0.0003	0.0041	0.0110	0.00005	0.0090	0.011	0.025	0.0012	0.000021	0.0003

Despite the fact that a purer ACH can be obtained at 95 °C, the results of the ACH yield and crystal size advocate the use of a low temperature (e.g., 0 °C) as optimal for the salting-out process.

3.2. ACH Calcination for SGA Production

To study ACH decomposition by calcination, a large number of ACH crystals were produced in an additional experiment using 200 mL of the liquor, T = 0 °C, and a duration of 1 h. Figure 6a shows the phase composition of the crystals obtained. It can be seen that the impurities did not form individual phases and were incorporated into the crystalline phase. Figure 6b shows the ACH crystal size distribution. The average ACH crystal size was 156.57 µm. Increasing the salting-out time leads to a significant increase in the crystal size. It can be seen from Figure 6c–d that surfaces of large particles >200 µm became nucleation sites for smaller ones. Some crystals were greater than 800 µm in size (Figure 6d).

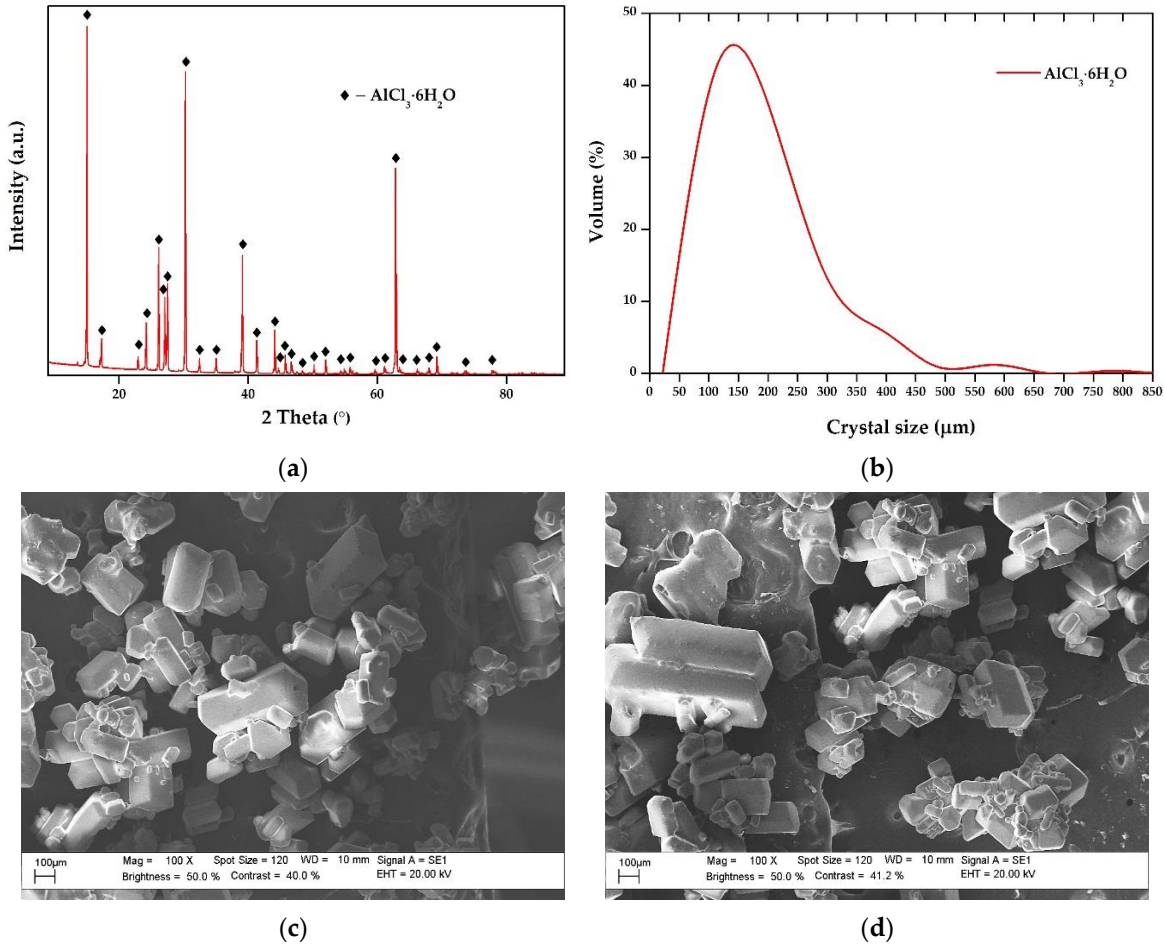

Figure 6. ACH crystals obtained at T_{liqour} = 0 °C, V_{liqour} = 200 mL, and duration 1 h: (**a**) XRD analysis; (**b**) distribution of the crystal size; (**c**) and (**d**) SEM images.

The TGA/DSC analysis was carried out in air atmosphere to determine the mass loss and main thermal effects present upon the heating of ACH. There are two endothermic peaks and one exothermic

peak shown in Figure 7. The first peak (before 100 °C) indicates the evaporation of physical water with a loss of ~1 wt.%. The second peak at 180 °C indicates ACH decomposition, which is accompanied by a loss of more than 78 wt.% from the total mass. Ivanov et al. [42] showed that this peak corresponds to the decomposition of ACH to Al_2O_3, H_2O, and HCl by the following reaction:

$$2AlCl_3{\cdot}6H_2O_{(s)} = Al_2O_{3(s)} + 6HCl_{(g)}\uparrow + 9H_2O_{(g)}\uparrow. \quad (3)$$

A small exothermic peak at 850 °C indicates the phase transformation of amorphous alumina into γ-Al_2O_3; a small peak at 950 °C can indicate the transformation of γ-Al_2O_3 into α-Al_2O_3 [43]. The process of ACH decomposition could only be completed above 250 °C, when the ACH phase became undetectable by XRD, while the Al-product could be transformed into amorphous alumina until the temperature reached ~850 °C, when the γ-Al_2O_3 phase appeared.

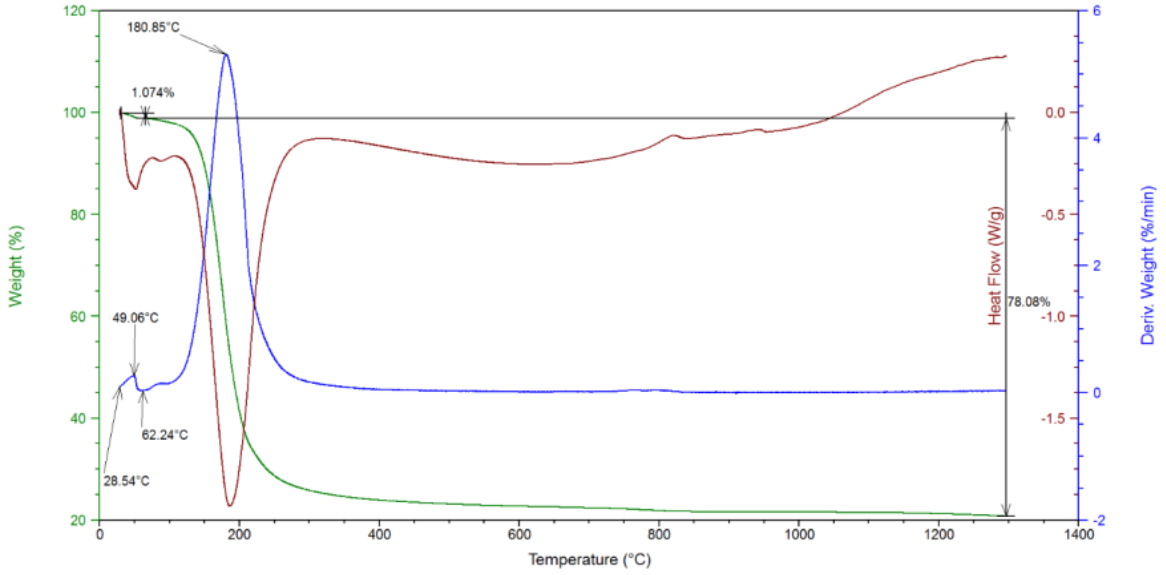

Figure 7. TGA/DSC curves of the $AlCl_3{\cdot}6H_2O$ sample at a heating rate of 5 °C/min from 28 to 1300 °C (initial mass of the sample: 43.374 mg; atmosphere: air; the green line shows the weight loss, the blue line shows the derivative of the weight change rate, and the red line shows the heat flow).

The direct production of sandy grade alumina (SGA-C) from ACH crystals was carried out by calcination at 1000 °C for 1 h. Using these technological parameters, it is possible to obtain SGA with the smallest chlorine content (less of 0.2 wt.%) [44] and a high specific surface (>60 m^2/g). A further increase of the temperature will result in a high content of α-Al_2O_3 and a decrease in the specific surface to less than 60 m^2/g [45].

3.3. ACH Calcination to Produce Amorphous ACH400

Further study will focus on producing amorphous ACH400 and obtaining sandy grade alumina from it. The idea is to remove chlorine and water from ACH, but to avoid the crystallization of alumina, which can occur at temperatures higher than 800 °C. It can be seen from Section 3.2 that the decomposition of ACH crystals into aluminum oxide via reaction (3) starts at temperatures of around 100–150 °C. However, the decomposition of ACH usually occurs in two steps: first, it decomposes into an aluminum oxychloride compound at temperatures up to 350 °C, which can be presented by the following reaction:

$$2AlCl_3{\cdot}6H_2O_{(s)} = Al_2(OH)_4Cl_2{\cdot}H_2O_{(s)} + 4HCl_{(g)}\uparrow + 7H_2O_{(g)}\uparrow, \quad (4)$$

and second, the aluminum oxychloride decomposes into Al_2O_3 at higher temperatures. However, if the heating rate is high enough, reactions (3) and (4) occur almost simultaneously (see, for example, [42]), and this results in one broad peak from 100 to 300 °C, as can be seen in Figure 7. In the present study, it was found that in order to maximize the removal of chlorine ions and thereby ACH400 formation, it is necessary to anneal ACH at temperatures above ~400 °C.

Taking into account the above, ACH400 was obtained by the calcination of ACH crystals at T = 400 °C for 1 h. This was further used to obtain sandy grade alumina (SGA-A) by a novel alkali treatment method described in Section 3.5.

3.4. Comparison of SGA-C and ACH400

This section provides a comparison of the sandy grade alumina (SGA-C) produced by high-temperature calcination and amorphous alumina (ACH400) produced by the low-temperature calcination of ACH crystals. The samples of Al_2O_3 obtained have different phase compositions, particle sizes, and forms (Figure 8). Figure 8a presents the results of XRD analysis of powders. It can be seen that the sample calcined at 400 °C is fully amorphous, while the sample calcined at 1000 °C contains crystalline phases, which are stable and metastable polymorphs of Al_2O_3. The main phase is found to be metastable γ-Al_2O_3, while the most stable form, corundum (α-Al_2O_3), does not exceed 10 wt.%. After low-temperature ACH calcination with the subsequent removal of H_2O and HCl, the particle size of the initial ACH crystals increases. As a result, ACH400 has an average particle size of 95.19 μm, while that of SGA-C calcined at 1000 °C is 43.67 μm (Figure 8b). Amorphous alumina powder retains an initial hexagonal shape of the particles similar to that of crystalline SGA-C (Figure 8c,d). The ACH400 particle surface partly remains smooth and is partly covered with long pores that are ~5 μm in length, which were formed when water and HCl were evaporated (Figure 8e). The SGA-C powder becomes brittle, and the entire surface of the SGA-C particles contains micro- and nanopores (Figure 8f).

The BET analysis of samples showed that the flat surface of the initial ACH crystals provides a low specific surface area of about 0.7 m^2/g. During ACH decomposition, pores appeared on the particle surface, which led to an increase of the specific surface area for ACH400 to 36.9 m^2/g. Further calcination at 1000 °C resulted in the entire surface of the particles consisting of pores, and the specific surface area for SGA-C increased to 71.2 m^2/g. Due to such a high specific surface area of the SGA-C obtained by the acid treatment, its dissolution rate in cryolite (Na_3AlF_6) was faster than the SGA obtained by the Bayer alkaline method [46].

The chemical composition of the initial ACH, ACH400, and SGA-C samples is shown in Table 3. It can be seen that the amount of impurities increases and the chlorine content decreases significantly when increasing the calcination temperature.

Table 3. The chemical composition, measured by ISP-OES, of impurities in ACH, amorphous alumina, and sandy grade alumina (wt.%).

Samples	Cr	Fe	K	Mn	Na	P	Si	Ti	V	Zn	Cl
ACH	0.0041	0.015	0.0081	0.0006	0.043	0.022	0.012	0.0094	0.00044	0.0002	-
ACH400	0.073	0.027	0.015	0.001	0.074	0.038	0.022	0.016	0.0008	0.0004	5.27
SGA-C	0.076	0.029	0.016	0.001	0.081	0.041	0.023	0.018	0.0009	0.0004	0.15

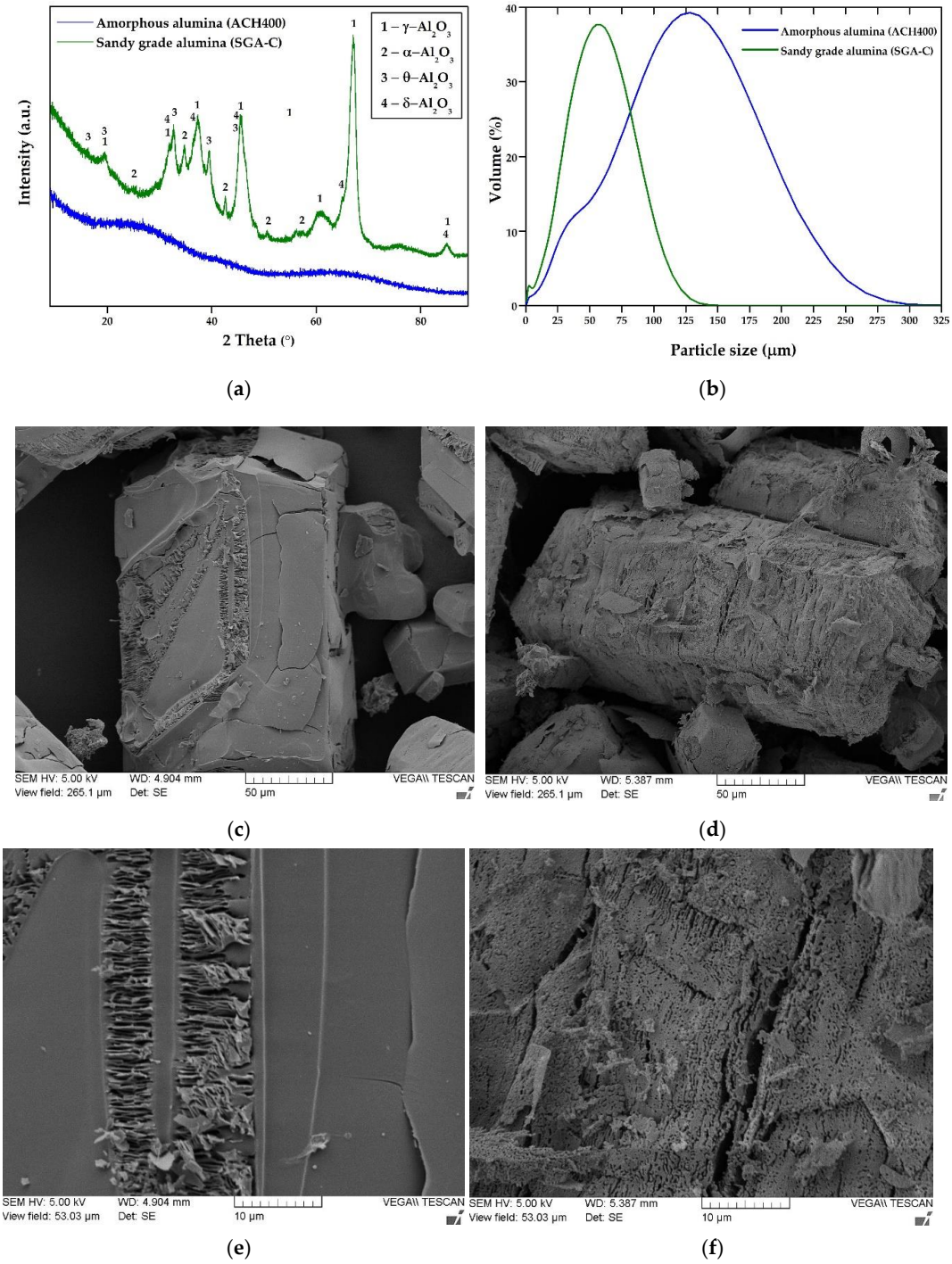

Figure 8. Data of ACH400 (T = 400 °C; τ = 1 h) and SGA-C (T = 1000 °C; τ = 1 h) obtained from ACH calcination: (**a**) XRD analysis; (**b**) distribution of the particle size; (**c**) and (**d**) SEM images of the particle shape for ACH400 and SGA-C powders, respectively; (**e**) and (**f**) SEM images of the particle surface for ACH400 and SGA-C powders, respectively.

3.5. SGA Production from Amorphous Alumina

The SGA-C obtained by the direct acid treatment has a high specific surface area; however, the particle shape and the content of impurities do not meet the technical standards accepted at RUSAL plants [44]. It is possible to reduce the impurities content, if recrystallization or solvent extraction methods are utilized [47].

Another approach involves alkaline treatment of the Al_2O_3 by the Bayer process [48]. In this case, Al_2O_3 from the acid treatment stage is first leached in an alkaline aluminate solution to obtain a liquor supersaturated by alumina. For this process, high-pressure leaching equipment should be used. It is also necessary to obtain the alkaline aluminate liquor with a caustic module (the molar ratio of Na_2O to Al_2O_3 in the solution) below 1.5 [49]. Then, the supersaturated alkaline aluminate liquor can enter a precipitation stage, where gibbsite ($Al(OH)_3$) precipitates out in the presence of a large number of seed crystals (to achieve that, the ratio of Al_2O_3 in the liquor to that in the seed crystals must be greater than 4). To obtain coarse particles of $Al(OH)_3$ (only 10% of particles should have a size below 45 μm) and a precipitation rate of more than 50% required for SGA production, the duration of the whole process should be 48–72 h [50]. Therefore, in order to produce SGA that suits the required standards, the use of high-pressure equipment and large decomposers, as well as additional energy and raw materials, is required, which significantly increases the cost of the final product.

It is also possible to apply the above alkaline recrystallization process at lower material/energy costs using an enlargement method [51] based on the difference in solubility of coarse particles of gibbsite or boehmite (AlOOH) and amorphous alumina (or highly dispersed hydroxide) [52,53]. Previous studies on the leaching of amorphous alumina in hot alkaline liquor have shown that, in this case, the process can occur at atmospheric pressure [54,55] and no high-pressure leaching equipment is necessary.

In this paper, we have proposed, for the first time, the use of the intermediate product of the acid treatment stage, the amorphous ACH400, in the alkaline recrystallization process. In the present research, the amorphous alumina obtained after the acid treatment stage was subjected to further alkaline treatment and subsequent recrystallization by the mother liquor and coarse $Al(OH)_3$ particles, respectively, formed during a stage of the Bayer process on the Ural Aluminum Plant (UAP). As a result, the amorphous alumina dissolved, increasing the supersaturation of the aluminate solution, which in turn led to the precipitation of aluminum hydroxide on the coarse $Al(OH)_3$ particles. Finally, the sandy grade alumina could be obtained after filtration and calcination. The proposed process flowsheet is shown in Figure 9.

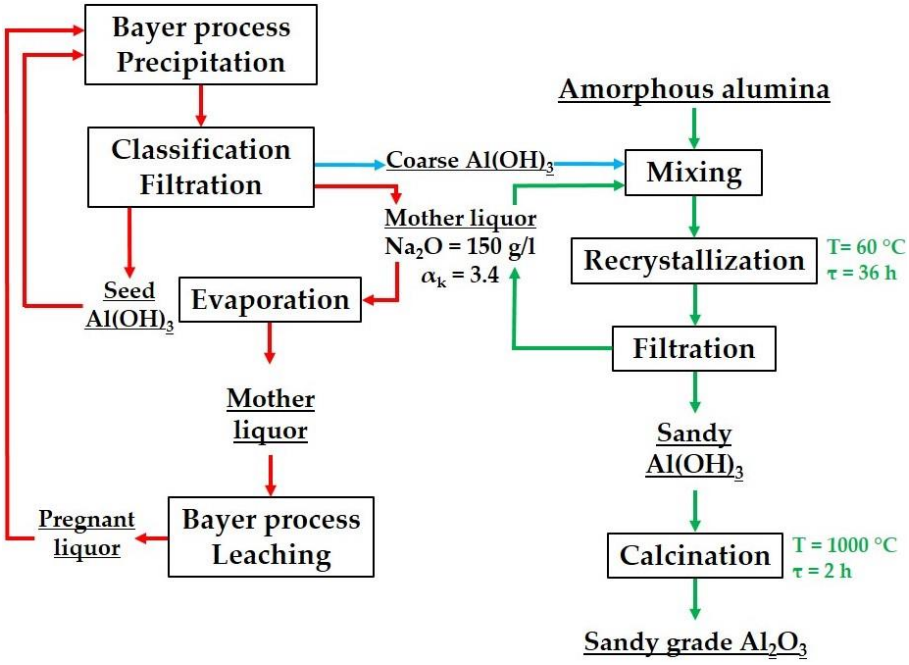

Figure 9. Flowsheet of SGA production from amorphous alumina obtained by low-temperature ACH calcination.

The results of the proposed treatment are discussed in the rest of the section. The particle size distribution of the initial $Al(OH)_3$ particles produced on the UAP and of $Al(OH)_3$ particles after the recrystallization stage is shown in Figure 10. The initial powder contains about 25% of a fraction of fewer than 50 µm, which prevents the production of SGA from this powder on the UAP. To increase the size of the coarse $Al(OH)_3$ particles, ACH400 powder was used. When mixed with an alkaline liquor, due to the high specific surface area (36.9 m^2/g for ACH400 and 0.1 m^2/g for coarse $Al(OH)_3$), it will be dissolved first, and then precipitated on the $Al(OH)_3$ surface. This process can be described by the following reactions:

$$Al_2O_{3(s)} + NaOH_{(l)} = NaAl(OH)_{4(l)}, \quad (5)$$

$$NaAl(OH)_{4(l)} + Al(OH)_{3(s)} = 2Al(OH)_{3(s)} + NaOH_{(l)}. \quad (6)$$

According to reaction (5), amorphous alumina is dissolved in the liquor to form hydrated sodium aluminate, thereby increasing the supersaturation of the liquor relative to the coarse $Al(OH)_3$ particles [52]. Next, dissolved alumina in the form of hydrated sodium aluminate precipitates on the surface of $Al(OH)_3$ via reaction (6). Li et al. showed that $Al(OH)_3$ agglomeration also proceeds during the late stages of the precipitation process [56]. It can be seen (Figure 10) that the particle size distribution after recrystallization shifted towards a greater average size and a higher volume fraction of coarse particles.

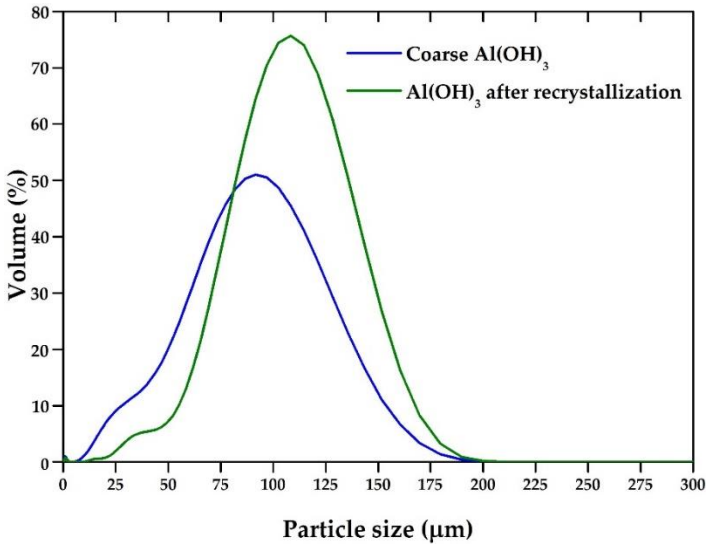

Figure 10. Distribution of particle size for coarse $Al(OH)_3$ and $Al(OH)_3$ after recrystallization.

Figure 11a–d shows a comparison of the morphology of the coarse $Al(OH)_3$ particles and $Al(OH)_3$ particles after recrystallization. Initially, the coarse $Al(OH)_3$ had a large number of small particles, for which the size was less than 20 µm (Figure 11a). The $Al(OH)_3$ sample after recrystallization mainly consisted of large particles with a size of 100–125 µm (Figure 11c); a large number of small particles were not found, as was the case before (Figure 11a). An analysis of the particle shape of the coarse $Al(OH)_3$ revealed voids and surface inhomogeneity (Figure 11b), whereas, after recrystallization, the $Al(OH)_3$ particles had an almost uniform structure of a dense pack of small particles, consisting of larger agglomerates (Figure 11d).

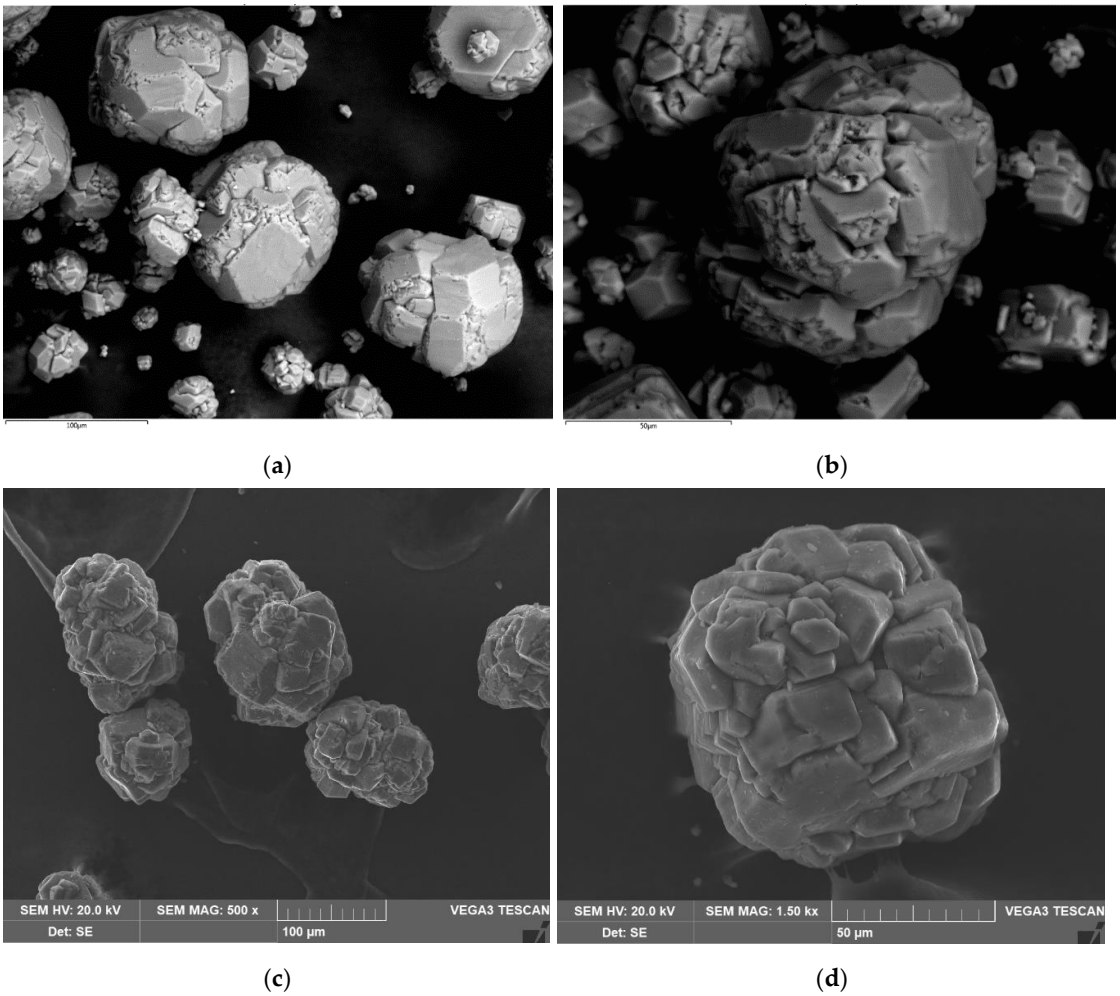

Figure 11. SEM images of (**a**,**b**) coarse $Al(OH)_3$ and (**c**,**d**) $Al(OH)_3$ after recrystallization.

The proposed process proceeds at atmospheric pressure and the liquor temperature of 60 °C. The Al_2O_3 precipitation degree after 36 h was only 4.5%. The XRD analysis shows that the powder obtained only consists of the gibbsite phase (Figure 12). The low Al_2O_3 precipitation degree and the absence of amorphous alumina in the recrystallized sample (Figure 11c) confirm that the growth of $Al(OH)_3$ occurs due to the leaching and recrystallization of ACH400 powder.

After filtration, the mother liquor was reused to leach a new portion of amorphous alumina. For SGA production, it is necessary to calcinate $Al(OH)_3$ at T = 1000 °C and τ = 1 h. The removal of external moisture and crystalline water in $Al(OH)_3$ occurs according to the following reaction:

$$2Al(OH)_{3(s)} = Al_2O_{3(s)} + 3H_2O_{(g)}\uparrow. \quad (7)$$

It can be seen from Figure 10 that the number of particles smaller than 45 µm becomes lower than 5%. Since calcination in this research was carried out in a muffle furnace, the attrition index (AI) was not studied. However, Wind et al. showed that decreasing the fraction of particles greater than 45 µm increases the AI in the calcination furnace [57]. Therefore, if the $Al(OH)_3$ after recrystallization contains 5% of particles smaller than 45 µm, the AI is 5%. This means that, even after abrasion, the obtained SGA-A must comply with the SGA requirements.

The XRD pattern of the SGA-C obtained after $Al(OH)_3$ calcination is shown in Figure 12. SGA-C consists of two phases: 95% γ-Al_2O_3 and 5% α-Al_2O_3.

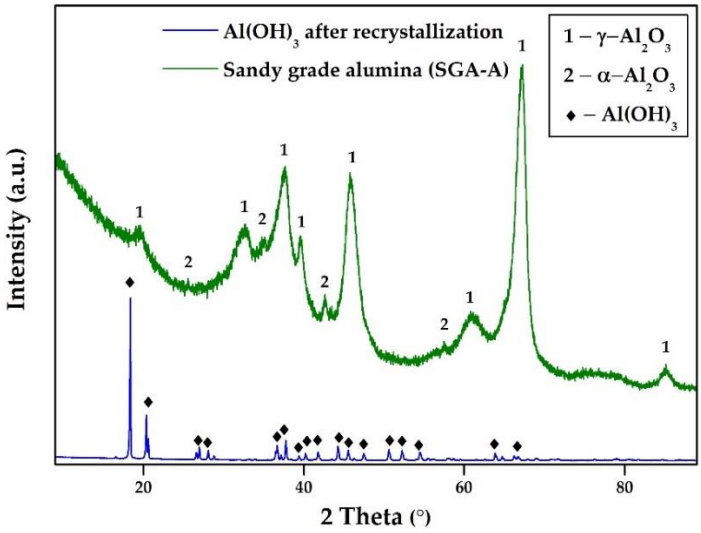

Figure 12. XRD analysis of $Al(OH)_3$ after the recrystallization process and SGA-A (T = 1000 °C, τ = 1 h).

The chemical composition of SGA-C is presented in Table 4. Since ACH400 was completely dissolved in the alkali liquor, the maximum dilution of impurities also occurred. Therefore, the chlorine content in the SGA-A was quite low. Senyuta et al. [48] showed that, in a real metallurgical process, chlorine can be accumulated in circulating liquors at the amount of 40–90 g/L, which may lead to an increase of the chlorine content in the SGA to about 0.013 wt.%.

Table 4. The chemical composition, measured by ISP-OES, of impurities in SGA-C (wt.%).

Cr_2O_3	Fe_2O_3	K_2O	MnO_2	Na_2O	P_2O_5	SiO_2	TiO_2	V_2O_5	ZnO	Cl
0.0005	0.01	0.008	0.0001	0.31	0.0009	0.003	0.002	0.0004	0.0001	0.004

Using the proposed novel process, it is possible to reduce the cost of SGA production, which is necessary for modern electrolysis processes. Acid/alkali treatment enables the leaching stage of the amorphous alumina at high pressure to be eliminated; the long precipitation time to be significantly shortened; and the sandy grade alumina, which is appropriate with regards to the SGA standards, to be produced.

4. Conclusions

In this work, a novel method has been developed for sandy grade alumina production from the Al-chloride liquor obtained by the HCl leaching of coal fly ash. In this method, the amorphous alumina obtained after traditional acid treatment of the Al liquor is subjected to alkaline treatment by the mother liquor from a Ural Aluminum Plant and to subsequent precipitation using the coarse $Al(OH)_3$ particles from UAP, with further calcination to obtain SGA suitable for metallic aluminum production. The following points concerning the technological parameters of various stages of the novel process can be made:

1. The temperature of the salting-out process affects the ACH crystal size and impurities content. At T = 0 and 95 °C, the total amount of impurities is 0.1 and 0.06 wt.%, and the average particle size is 85 and 135 μm, respectively;
2. ACH calcination at T = 400 °C produces amorphous alumina with the specific surface of 36.9 m^2/g and content of chlorine ions of 5.27 wt.%;
3. ACH calcination at T = 1000 °C allows SGA production with the specific surface area of 71.2 m^2/g and chlorine ion content of 0.15 wt.%;

4. Alkaline recrystallization of amorphous alumina obtained after the calcination of ACH at 400 °C at T = 60 °C and Na_2O = 150 g/L, allows the average particle size of coarse $Al(OH)_3$ to be increased from 76 to 99 microns;
5. The calcination of recrystallized $Al(OH)_3$ at T = 1000 °C and maintenance for 1 h allows SGA with a content of chlorine ions of 0.004 wt.% to be obtained.

Author Contributions: Conceptualization, D.V., A.S., and A.K.; formal analysis, A.M.; funding acquisition, D.V.; investigation, D.V. and A.S.; project administration, D.V.; resources, D.V.; writing—original draft, D.V., A.S., and A.K.; writing—review and editing, D.V., A.S., and A.K. All authors have read and agreed to the published version of the manuscript.

Funding: This work was financially supported by the Russian Science Foundation Project No. 18-79-00305.

Acknowledgments: The authors would like to appreciate the assistance provided by The Center for Collective Use Testing Analytical Center of the JSC "Scientific-research institute of chemical technology" and that personally given to Natalya Ognevskaya for the chemical analysis of solid and liquid samples.

Conflicts of Interest: The authors declare no conflicts of interest.

References

1. Anawar, H.M.; Strezov, V.; Adyel, T.M.; Ahmed, G. Sustainable and Economically Profitable Reuse of Bauxite Mining Waste with Life Cycle Assessment. In *Sustainable and Economic Waste Management Resource Recovery Techniques*; Anawar, H.M., Strezov, V., Abhilash, Eds.; CRC Press: Boca Raton, MA, USA, 2019; p. 328. ISBN 9780429279072.
2. Smith, P. The processing of high silica bauxites - Review of existing and potential processes. *Hydrometallurgy* **2009**, *98*, 162–176. [CrossRef]
3. Senyuta, A.; Panov, A.; Suss, A.; Layner, Y. Innovative Technology for Alumina Production from Low-Grade Raw Materials. In *Light Metals 2013*; Springer: Cham, Switzerland, 2013; pp. 203–208. ISBN 978-3-319-65136-1.
4. Chen, J.; Li, X.; Cai, W.; Shi, Y.; Hui, X.; Cai, Z.; Jin, W.; Fan, J. High-efficiency extraction of aluminum from low-grade kaolin via a novel low-temperature activation method for the preparation of poly-aluminum-ferric-sulfate coagulant. *J. Clean. Prod.* **2020**, *257*, 120399. [CrossRef]
5. Brichkin, V.N.; Kurtenkov, R.V.; Eldeeb, A.B.; Bormotov, I.S. State and development options for the raw material base of aluminum in non-bauxite regions. *Obogashchenie Rud* **2019**, *2019*, 31–37. [CrossRef]
6. Barry, T.S.; Uysal, T.; Birinci, M.; Erdemoğlu, M. Thermal and Mechanical Activation in Acid Leaching Processes of Non-bauxite Ores Available for Alumina Production—A Review. *Mining, Metall. Explor.* **2019**, *36*, 557–569. [CrossRef]
7. Zinoveev, D.V.; Grudinskii, P.I.; Dyubanov, V.G.; Kovalenko, L.V.; Leont'ev, L.I. Global recycling experience of red mud—A review. Part i: Pyrometallurgical methods. *Izv. Ferr. Metall.* **2018**, *61*, 843–858. [CrossRef]
8. Gao, Y.; Liang, K.; Gou, Y.; Wei, S.; Shen, W.; Cheng, F. Aluminum extraction technologies from high aluminum fly ash. *Rev. Chem. Eng.* **2020**. [CrossRef]
9. Mahinroosta, M.; Allahverdi, A. Enhanced alumina recovery from secondary aluminum dross for high purity nanostructured γ-alumina powder production: Kinetic study. *J. Environ. Manage.* **2018**, *212*, 278–291. [CrossRef]
10. Yang, Q.; Li, Q.; Zhang, G.; Shi, Q.; Feng, H. Investigation of leaching kinetics of aluminum extraction from secondary aluminum dross with use of hydrochloric acid. *Hydrometallurgy* **2019**, *187*, 158–167. [CrossRef]
11. Ding, J.; Ma, S.; Shen, S.; Xie, Z.; Zheng, S.; Zhang, Y. Research and industrialization progress of recovering alumina from fly ash: A concise review. *Waste Manag.* **2017**, *60*, 375–387. [CrossRef]
12. Wang, Y.; Zhang, T.; Lyu, G.; Guo, F.; Zhang, W.; Zhang, Y. Recovery of alkali and alumina from bauxite residue (red mud) and complete reuse of the treated residue. *J. Clean. Prod.* **2018**, *188*, 456–465. [CrossRef]
13. Project Energy Strategy of the Russian Federation for the Period Until 2035. Available online: https://minenergo.gov.ru/node/1920 (accessed on 18 December 2019).
14. Shi, Y.; Jiang, K.-X.; Zhang, T.-A. A cleaner electrolysis process to recover alumina from synthetic sulfuric acid leachate of coal fly ash. *Hydrometallurgy* **2020**, *191*, 105196. [CrossRef]
15. Wu, Y.; Yang, X.; Li, L.; Wang, Y.; Li, M. Kinetics of extracting alumina by leaching coal fly ash with ammonium hydrogen sulfate solution. *Chem. Pap.* **2019**, *73*, 2289–2295. [CrossRef]

16. Guo, C.; Zou, J.; Ma, S.; Yang, J.; Wang, K. Alumina extraction from coal fly ash via low-temperature potassium bisulfate calcination. *Minerals* **2019**, *9*, 585. [CrossRef]
17. Ma, Z.; Zhang, S.; Zhang, H.; Cheng, F. Novel extraction of valuable metals from circulating fluidized bed-derived high-alumina fly ash by acid–alkali–based alternate method. *J. Clean. Prod.* **2019**, *230*, 302–313. [CrossRef]
18. Zhang, Y.; Li, M.; Liu, D.; Hou, X.; Zou, J.; Ma, X.; Shang, F.; Wang, Z. Aluminum and iron leaching from power plant coal fly ash for preparation of polymeric aluminum ferric chloride. *Environ. Technol. (United Kingd.)* **2019**, *40*, 1568–1575. [CrossRef]
19. Huang, J.; Wang, Y.; Zhou, G.; Gu, Y. Investigation on the Effect of Roasting and Leaching Parameters on Recovery of Gallium from Solid Waste Coal Fly Ash. *Metals (Basel)* **2019**, *9*, 1251. [CrossRef]
20. Li, G.; Ye, Q.; Deng, B.; Luo, J.; Rao, M.; Peng, Z.; Jiang, T. Extraction of scandium from scandium-rich material derived from bauxite ore residues. *Hydrometallurgy* **2018**, *176*, 62–68. [CrossRef]
21. Pan, J.; Nie, T.; Vaziri Hassas, B.; Rezaee, M.; Wen, Z.; Zhou, C. Recovery of rare earth elements from coal fly ash by integrated physical separation and acid leaching. *Chemosphere* **2020**, *248*, 126112. [CrossRef]
22. Wu, L.; Zhao, J.; Xue, F.; Cheng, H.; Cheng, F. Phase equilibrium andseparation of $AlCl_3$-$FeCl_3$-HCl-H_2Osystem [$AlCl_3$-$FeCl_3$-HCl-H_2O 体系的相平衡及相分离]. *Guocheng Gongcheng Xuebao/The Chin. J. Process Eng.* **2020**, *20*, 318–323.
23. Long, W.; Ting-An, Z.; Guozhi, L.; Weiguang, Z.; Yan, L.; Zhihe, D.; Liping, N. A new green process to produce activated alumina by spray pyrolysis. *Green Process. Synth.* **2018**, *7*, 464–469. [CrossRef]
24. Cheng, H.; Wu, L.; Zhang, J.; Lv, H.; Guo, Y.; Cheng, F. Experimental investigation on the direct crystallization of high-purity $AlCl_3{\cdot}6H_2O$ from the $AlCl_3$-NaCl-H_2O(-HCl-C_2H_5OH) system. *Hydrometallurgy* **2019**, *185*, 238–243. [CrossRef]
25. Yu, X.; Liu, M.; Zheng, Q.; Chen, S.; Zou, F.; Zeng, Y. Measurement and Correlation of Phase Equilibria of Ammonium, Calcium, Aluminum, and Chloride in Aqueous Solution at 298.15 K. *J. Chem. Eng. Data* **2019**, *64*, 3514–3520. [CrossRef]
26. Yu, X.; Zheng, Q.; Wang, L.; Liu, M.; Cheng, X.; Zeng, Y. Solid-liquid phase equilibrium determination and correlation of ternary systems NH_4Cl+$AlCl_3$+H_2O, $MgCl_2$+$AlCl_3$+H_2O and $SrCl_2$+$AlCl_3$+H_2O at 298 K. *Fluid Phase Equilib.* **2020**, *507*, 112426. [CrossRef]
27. Mahinroosta, M.; Allahverdi, A. A promising green process for synthesis of high purity activated-alumina nanopowder from secondary aluminum dross. *J. Clean. Prod.* **2018**, *179*, 93–102. [CrossRef]
28. Guo, Y.; Yang, X.; Cui, H.; Cheng, F.; Yang, F. Crystallization behavior of $AlCl_3{\cdot}6H_2O$ in hydrochloric system. *Huagong Xuebao/CIESC J.* **2014**, *65*, 3960–3967.
29. Valeev, D.; Kunilova, I.; Alpatov, A.; Mikhailova, A.; Goldberg, M.; Kondratiev, A. Complex utilisation of ekibastuz brown coal fly ash: Iron & carbon separation and aluminum extraction. *J. Clean. Prod.* **2019**, *218*, 192–201.
30. Valeev, D.; Kunilova, I.; Alpatov, A.; Varnavskaya, A.; Ju, D. Magnetite and carbon extraction from coal fly ash using magnetic separation and flotation methods. *Minerals* **2019**, *9*, 320. [CrossRef]
31. Sturges, H.A. The Choice of a Class Interval. *J. Am. Stat. Assoc.* **1926**, *21*, 65–66. [CrossRef]
32. Miles, G.L. Some Studies in the System $AlCl_3$-$FeCl_3$-KCl-NaCl-HCl-H_2O at 25, 30 an4 35°. *J. Am. Chem. Soc.* **1947**, *69*, 1716–1719. [CrossRef]
33. Guo, Y.; Lv, H.; Yang, X.; Cheng, F. $AlCl_3{\cdot}6H_2O$ recovery from the acid leaching liquor of coal gangue by using concentrated hydrochloric inpouring. *Sep. Purif. Technol.* **2015**, *151*, 117–183. [CrossRef]
34. Christov, C.; Dickson, A.G.; Moller, N. Thermodynamic modeling of aqueous aluminum chemistry and solid-liquid equilibria to high solution concentration and temperature. I. the acidic H-Al-Na-K-Cl-H_2O system from 0 to 100∈°C. *J. Solution Chem.* **2007**, *36*, 1495–1523. [CrossRef]
35. Cheng, H.; Wu, L.; Cao, L.; Zhao, J.; Xue, F.; Cheng, F. Phase Diagram of $AlCl_3$-$FeCl_3$-H_2O(-HCl) Salt Water System at 298.15 K and Its Application in the Crystallization of $AlCl_3{\cdot}6H_2O$. *J. Chem. Eng. Data* **2019**, *64*, 5089–5094. [CrossRef]
36. Pak, V.I.; Kirov, S.S.; Mamzurina, O.I.; Nalivayko, A.Y. Understanding the regularities of aluminum chloride hexahydrate crystallization from hydrochloric acid solutions resultant from leaching of Russian kaolin clays. Part 1. process kinetics. *Tsvetnye Met.* **2020**, *2020*, 47–53. [CrossRef]
37. Golubev, V.O.; Chistyakov, D.G.; Brichkin, V.N.; Postika, M.F. Population balance of aluminate solution decomposition: Physical modelling and model setup. *Tsvetnye Met.* **2019**, *2019*, 75–81. [CrossRef]

38. Li, Y.; Zhang, Y.; Yang, C.; Zhang, Y. Precipitating sandy aluminium hydroxide from sodium aluminate solution by the neutralization of sodium bicarbonate. *Hydrometallurgy* **2009**, *98*, 52–57. [CrossRef]
39. Elduayen-Echave, B.; Lizarralde, I.; Larraona, G.S.; Ayesa, E.; Grau, P. A New Mass-Based Discretized Population Balance Model for Precipitation Processes: Application to Struvite Precipitation. *Water Res.* **2019**, *155*, 26–41. [CrossRef]
40. Li, J.; Addai-Mensah, J.; Thilagam, A.; Gerson, A.R. Growth mechanisms and kinetics of gibbsite crystallization: Experimental and quantum chemical study. *Cryst. Growth Des.* **2012**, *12*, 3096–3103. [CrossRef]
41. Gao, W.; Li, Z.; Asselin, E. Solubility of $AlCl_3{\cdot}6H_2O$ in the Fe(II) + Mg + Ca + K + Cl + H_2O system and its salting-out crystallization with $FeCl_2$. *Ind. Eng. Chem. Res.* **2013**, *52*, 14282–14290. [CrossRef]
42. Ivanov, V.V.; Kirik, S.D.; Shubin, A.A.; Blokhina, I.A.; Denisov, V.M.; Irtugo, L.A. Thermolysis of acidic aluminum chloride solution and its products. *Ceram. Int.* **2013**, *39*, 3843–3848. [CrossRef]
43. Zhang, N.; Yang, Y.; Wang, Z.; Shi, Z.; Gao, B.; Hu, X.; Tao, W.; Liu, F.; Yu, J. Study on the thermal decomposition of aluminium chloride hexahydrate. *Can. Metall. Q.* **2018**, *57*, 235–244. [CrossRef]
44. Suss, A.; Senyuta, A.; Kravchenya, M.; Smirnov, A.; Panov, A. The quality of alumina produced by the hydrochloric acid process and potential for improvement. In Proceedings of the The International Committee for Study of Bauxite, Alumina & Aluminium (ICSOBA), Dubai, UAE, 29 November 2015; Volume 44, pp. 1–8.
45. Zhao, L. Calcination of aluminum chloride hexahydrate (ach) for alumina production: Implications for alumina extraction from aluminum rich fly ash (ARFA). *Arch. Metall. Mater.* **2018**, *63*, 235–240.
46. Pak, V.I.; Kirov, S.S.; Nalivaiko, A.Y.; Ozherelkov, D.Y.; Gromov, A.A. Obtaining alumina from kaolin clay via aluminum chloride. *Materials (Basel).* **2019**, *12*, 3938. [CrossRef] [PubMed]
47. Cui, L.; Cheng, F.; Zhou, J. Preparation of high purity $AlCl_3{\cdot}6H_2O$ crystals from coal mining waste based on iron(III) removal using undiluted ionic liquids. *Sep. Purif. Technol.* **2016**, *167*, 45–54. [CrossRef]
48. Senyuta, A.; Panov, A.; Milshin, O.; Slobodyanyuk, E.; Smirnov, A. *Method for Producing Metallurgical Alumina (Variants)*; Rospatent: Moscow, Russia, 2016; p. 20.
49. Panias, D.; Asimidis, P.; Paspaliaris, I. Solubility of boehmite in concentrated sodium hydroxide solutions: Model development and assessment. *Hydrometallurgy* **2001**, *59*, 15–29. [CrossRef]
50. Çelikel, B.; Demir, G.K.; Kayacl, M.; Baygul, M.; Suarez, C.E. Precipitation area upgrade at ETI aluminum. In *Light Metals*; Suarez, C.E., Ed.; Springer: Cham, Switzerland, 2012; pp. 129–133.
51. Liu, G.; Li, Z.; Qi, T.; Li, X.; Zhou, Q.; Peng, Z. Two-Stage Process for Precipitating Coarse Boehmite from Sodium Aluminate Solution. *JOM* **2017**, *69*, 1888–1893. [CrossRef]
52. Li, X.-B.; Yan, L.; Zhao, D.-F.; Zhou, Q.-S.; Liu, G.-H.; Peng, Z.-H.; Yang, S.-S.; Qi, T.-G. Relationship between $Al(OH)_3$ solubility and particle size in synthetic Bayer liquors. *Trans. Nonferrous Met. Soc. China (Engl. Ed.)* **2013**, *23*, 1472–1479. [CrossRef]
53. Li, H.; Addai-Mensah, J.; Thomas, J.C.; Gerson, A.R. The influence of Al(III) supersaturation and NaOH concentration on the rate of crystallization of $Al(OH)_3$ precursor particles from sodium aluminate solutions. *J. Colloid Interface Sci.* **2005**, *286*, 511–519. [CrossRef]
54. Alex, T.C.; Kumar, R.; Roy, S.K.; Mehrotra, S.P. Mechanical Activation of Al-oxyhydroxide Minerals—A Review. *Miner. Process. Extr. Metall. Rev.* **2016**, *37*, 1–26. [CrossRef]
55. Alex, T.C.; Kumar, R.; Roy, S.K.; Mehrotra, S.P. Towards ambient pressure leaching of boehmite through mechanical activation. *Hydrometallurgy* **2014**, *144–145*, 99–106. [CrossRef]
56. Li, X.-B.; Feng, G.-T.; Zhou, Q.-S.; Peng, Z.-H.; Liu, G.-H. Phenomena in late period of seeded precipitation of sodium aluminate solution. *Trans. Nonferrous Met. Soc. China (Engl. Ed.)* **2006**, *16*, 947–950. [CrossRef]
57. Wind, S.; Raahauge, B.E. Experience with commissioning new generation gas suspension calciner. *Miner. Met. Mater. Ser.* **2016**, 155–162.